Special Issue of the 8th International Advances in Applied Physics and Materials Science Congress (APMAS 2018)

Estimation of C Solubility at SiC Saturation from the Reaction of Carbon Crucible with Si–Cr Solvent for Top-Seeded Solution Growth

K. Hyun[a], S.J. Kim[b] and T. Taishi[c,d,*]

[a]Mokpo National Maritime University, Division of Naval Officer Science, Mokpo, Korea
[b]Mokpo National Maritime University, Division of Marine Engineering, Mokpo, Korea
[c]Shinshu University, Faculty of Engineering, Nagano, Japan
[d]Shinshu University, Center for Energy and Environmental Science, Nagano, Japan

The reaction between a carbon crucible and Si–Cr solvent, and the carbon solubility at SiC saturation in Si–Cr solvent were investigated using infrared absorption after combustion, field-emission scanning electron microscopy, and electron probe microanalysis. $Si_{0.6}Cr_{0.4}$, commonly used for silicon carbide crystal growth, was maintained in a carbon crucible at 1500–1950 °C for several minutes. The amount of carbon dissolved in the solvent was determined. The carbon content initially increased for 5 min, then remained constant until 10th min, and finally increased again with time at high temperature. According to microanalysis, the second increase in carbon content was due to the crystallization of small SiC grains in the solvent after reaching saturation, while the constant carbon content was due to the equilibrium between the SiC interlayer along the crucible wall and the solvent. Assuming the plateau of carbon content closely represented the carbon solubility at each temperature, a pseudo binary phase diagram was created for Si and C. Experimentally obtained constant carbon contents is in good agreement with the carbon solubilities calculated using CALPHAD.

DOI: 10.12693/APhysPolA.135.1012

PACS/topics: silicon carbide, single crystal growth, top-seeded solution growth, growth rate, carbon solubility

1. Introduction

The 4H-SiC polytype of silicon carbide has received much attention as an alternative material that overcomes the limitations of silicon (Si) in high-power devices with low on-resistance [1]. This is due to SiC having 10 times the dielectric breakdown field strength, triple the band gap, and triple the thermal conductivity of Si. Furthermore, both *p*- and *n*-type SiC semiconductors can be fabricated.

Presently, physical vapor transport (PVT) techniques, such as sublimation above 2000 °C, are commonly used to grow bulk crystals of SiC [2]. The largest SiC wafer to date (6 inches) was prepared using the PVT method. Nevertheless, SiC produced using the PVT method has many defects, and its commercial production is uneconomical owing to the high temperature required for growth. Accordingly, further development of this growth technique is important.

Recently, a top-seeded solution growth (TSSG) method, in which a SiC seed is dipped into a solution in a carbon crucible as the carbon source, has been studied as a promising growth technique for obtaining micropipe-free wafers with low dislocation densities [3, 4]. As the temperature required in the TSSG method is lower than that used in PVT, a higher quality crystal is produced owing to the dynamic equilibrium at the solid–liquid interface [5].

During solution growth of SiC, the carbon content in the solvent increases with time, eventually reaching carbon saturation in the solvent. However, the SiC growth rate using the TSSG method is too slow owing to the low solubility of carbon in the Si melt, which is a key parameter affecting solution growth. Typically, transition metals, such as Cr, Ti, Fe, Al, and Ge, have been used to enhance carbon solubility, resulting in a high SiC growth rate in Si–metal systems [4, 6–9]. Among these multicomponent systems, a Si–Cr-based solvent has yielded the highest reported growth rate (2 mm/h) [10]. Carbon solubility is also related to the degree of supersaturation in the solution growth of SiC. Generally, increased carbon solubility leads to less supersaturation, resulting in ideal step-flow growth without unstable two-dimensional nucleation.

Theoretically calculated carbon solubilities in Si–Cr solvents have been reported using CALPHAD (calculation of phase diagrams) methods and have been relied upon in the solution growth of SiC [3, 10–12]. CALPHAD is a useful method for assigning a number to carbon solubility in a multicomponent system. However, an increasing number of components results in difficult and complex calculations that require a large amount of information, such as the thermodynamic properties of several components. Therefore, a facile experimental technique for determining carbon solubility would be useful because

*corresponding author; e-mail: taishi@shinshu-u.ac.jp

a detailed investigation based on experimental data for carbon solubility would be indispensable for growing 4H-SiC crystals with higher growth rates and improved crystal quality.

In this study, the increase in carbon content during the reaction between the carbon crucible and Si–Cr solvent was measured using infrared adsorption after combustion. From such experimental results, the carbon solubility at SiC saturation in the Si–Cr solvent was discussed.

2. Experimental procedure

Figure 1 is a schematic diagram of the experimental apparatus (MR39-H/D, Advance Riko, Japan) used in the furnace system. The setup consisted of a gold-coated furnace chamber, automatic temperature controller, two halogen lamps, and a thermocouple. In this study, the carbon crucible (IGS-744, Nippon Techno-Carbon, Japan) was used. Because we would like to evaluate the carbon solubility considered an interaction between the solvent and the carbon crucible which has been used to actual experiment of SiC crystal growth. A carbon crucible with a 6-mm inner diameter and 10-mm depth served as both container and carbon source. In each trial, a mixture of solvent materials ($Si_{0.6}Cr_{0.4}$, total of 0.3 g) was placed in the carbon crucible, using silicon (Si, 11N purity) and chromium (Cr, 99.9% purity) purchased from commercial suppliers (Tokuyama Corp. and Kojundo-Kagaku Laboratory, Japan, respectively). The carbon crucible was then placed on the thermocouple, as shown in Fig. 1. Prior to heating, the furnace chamber was flushed with high-purity Ar (99.9995%) for 2 h to minimize the presence of oxygen. The carbon crucible was heated to 1600 and 1800 °C using spot-focused infrared light from both halogen lamps. After the solvents had melted, the temperature was maintained for 1–60 min under an Ar atmosphere to determine the time required for carbon saturation. After heat treatment, the solvent was quenched and separated from the carbon crucible by decomposition in air at 900 °C for 2 h. The separated solvent was washed with distilled water in an ultrasonic cleaner, dried in a vacuum dryer at 120 °C for 24 h, and ground to a powder. The carbon content of the powdered solvent, containing no pieces of the carbon crucible, was measured by infrared absorption after combustion using a carbon and sulfur analyzer (EMIA-920V, Horiba, Japan). An EMIA-920V analyzer was used to measure carbon extracted during combustion in a programmable high-frequency furnace. The carbon in the sample was converted to carbon monoxide (CO) and/or carbon dioxide (CO_2) by combustion in a stream of oxygen gas, and the products were monitored and measured over time by infrared absorption. The carbon content was automatically calculated as percentage concentrations according to JIS G1211-3 and ISO 15350, including corrections for the blank and sample weight.

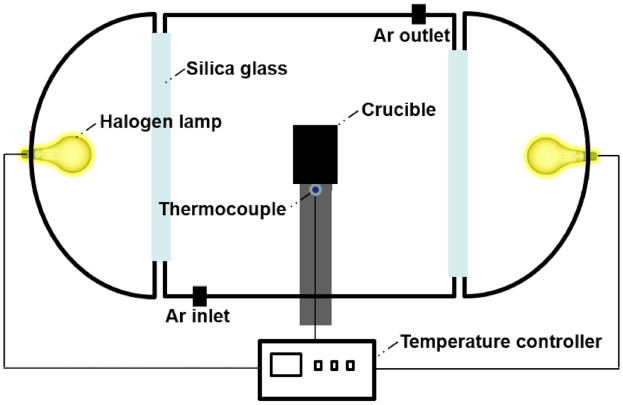

Fig. 1. Schematic diagram of experimental apparatus.

Microstructure and elemental composition analyses were performed using field-emission scanning electron microscopy with energy dispersive spectroscopy (FE-SEM/EDS, JEOL JSM-7800F, Japan) at an accelerating voltage of 11 kV, and electron probe microanalysis (EPMA, JEOL JXG-88R, Japan)

3. Results and discussion

Figure 2 shows the relationship between the carbon content in $Si_{0.6}Cr_{0.4}$ solvent and time at 1600, 1700, and 1800 °C. In general, the carbon content at 1800 °C was higher than that at 1600 °C. At 1800 °C, the carbon content initially increased for 5 min and then, having reached about 3.4 at%, became constant until 10 min, after which it significant increased again with time. Similar trends in changing carbon content were observed at 1600 °C and 1700 °C. Generally, a large amount of solute was dissolved in the solvent. The solute content in the solvent is known to increase before becoming constant after reaching saturation, with the constant value regarded as the solubility. However, in this study, the carbon content increased again after reaching a constant value.

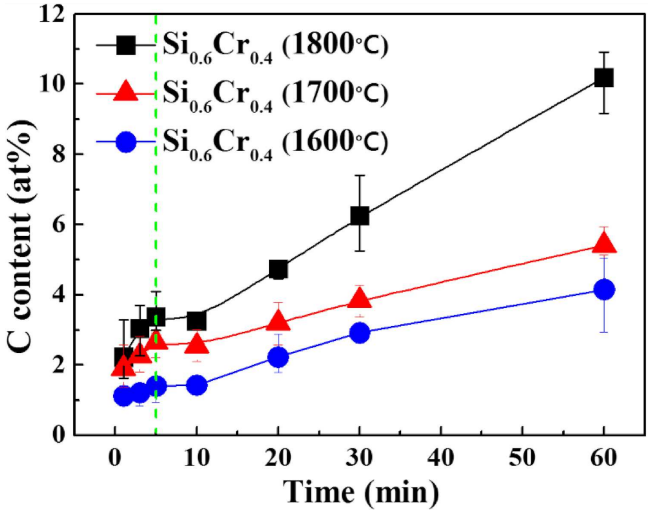

Fig. 2. Relationship between $Si_{0.6}Cr_{0.4}$ carbon content and time at 1600, 1700, and 1800 °C.

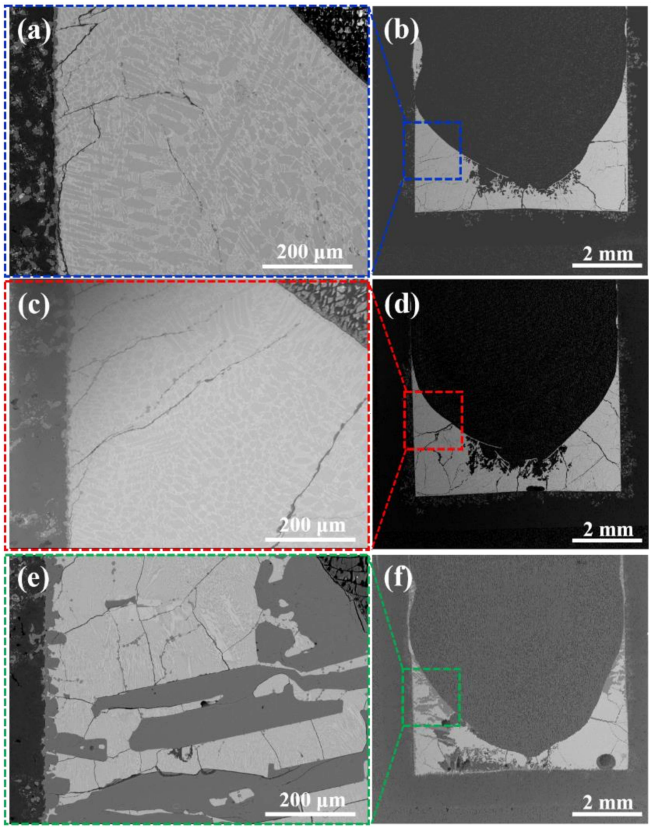

Fig. 3. Cross-sectional SEM (backscattered electron) images of carbon crucible after experiments with durations of (a, b) 1 min, (c, d) 5 min, and (e, f) 1 h at 1800 °C.

Figure 3 shows cross-sectional SEM (backscattered electron) images of carbon crucibles after experiments for 1 min (Fig. 3a and b), 3 min (Fig. 3c and d), and 1 h (Fig. 3e and f) at 1800 °C. In particular, SiC grains were only detected in the solvent used in the experiment for 1 h, as shown in Fig. 3e and f.

Figure 4 presents the EPMA elemental distribution mapping of the carbon crucibles after an experiment for 1 h at 1800 °C: (a) SEM (backscattered electron) image, (b) concentration mapping for carbon, (c) concentration scales (max/min levels) of carbon, (d) concentration mapping for Si, (e) concentration mapping for Cr, and (f) concentration scales (max/min levels) of Si and Cr.

EPMA mapping showing the relative distributions of C and Si clearly demonstrated the existence of SiC grains in the solvent, which were concentrated in the top half of the solvent. A gray level intensity in the backscattered electron images was interpreted as being directly correlated to the relative differences in atomic number or relative density (higher atomic numbers and densities led to more backscattered electrons). In other words, the density of the SiC grains was lower than that of the solvent, resulting in the SiC grains being concentrated in the top half of the solvent.

Figures 5 and 6 show the EPMA elemental distribution mapping near the carbon crucibles after experiments for 5 min and 1 h at 1800 °C: (a) SEM (backscattered electron) image, (b) concentration mapping for carbon, (c) concentration scales (max/min levels) of carbon, (d) concentration mapping for Si, (e) concentration mapping for Cr, and (f) concentration scales

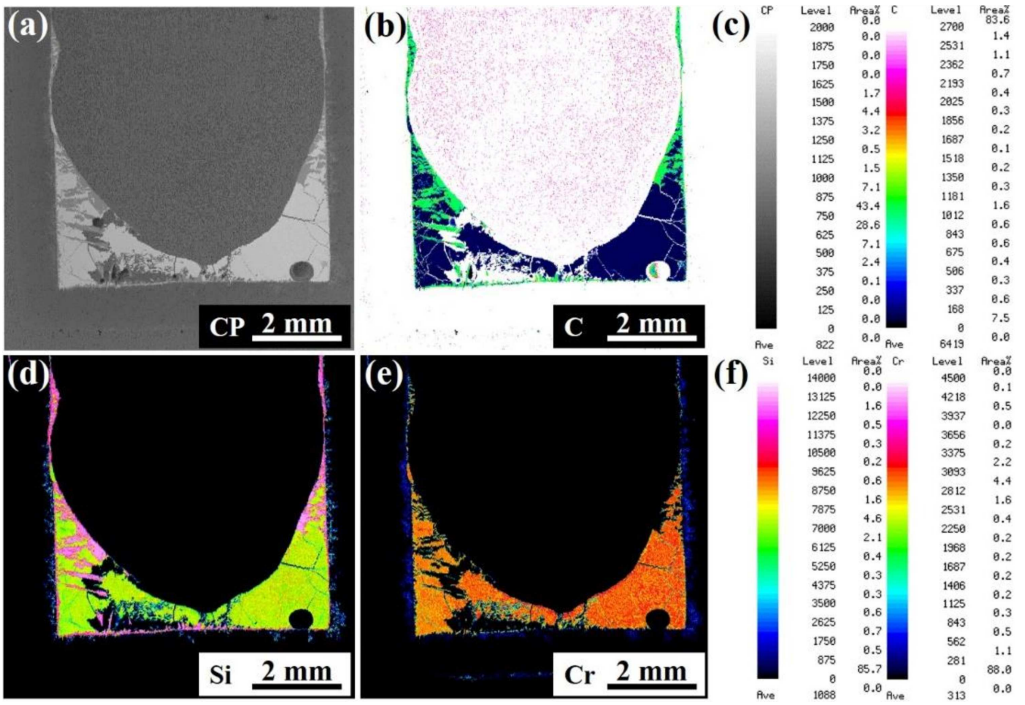

Fig. 4. Cross-sectional SEM (backscattered electron) image and EPMA elemental concentration mapping of the carbon crucible after an experiment for 1 h at 1800 °C.

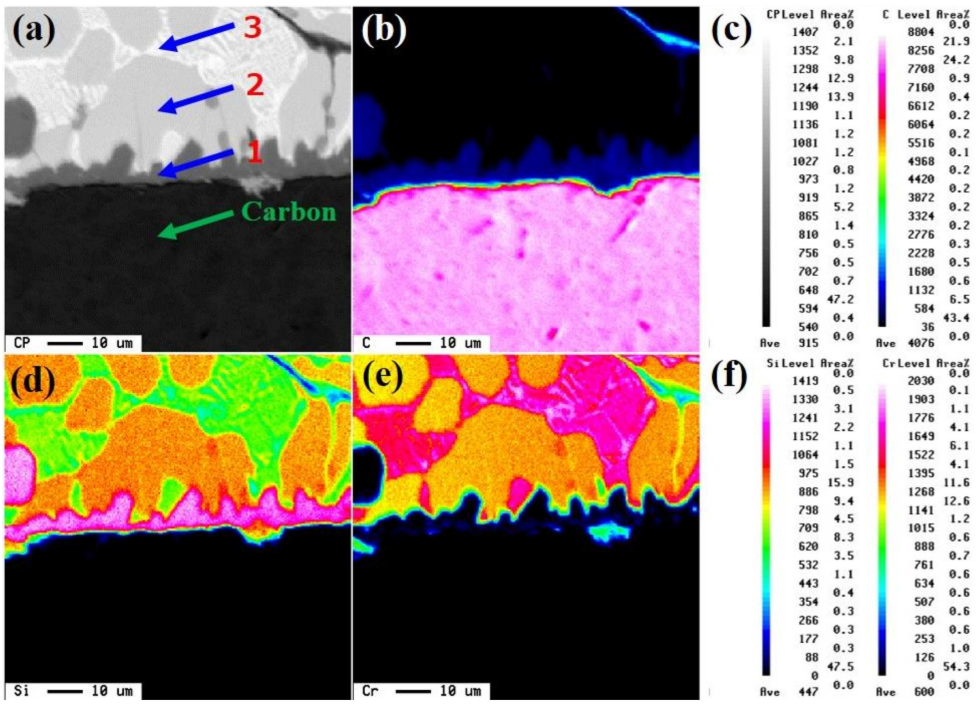

Fig. 5. Cross-sectional SEM (backscattered electron) images and EPMA elemental concentration mapping of the carbon crucible after experiments for 5 min at 1800 °C.

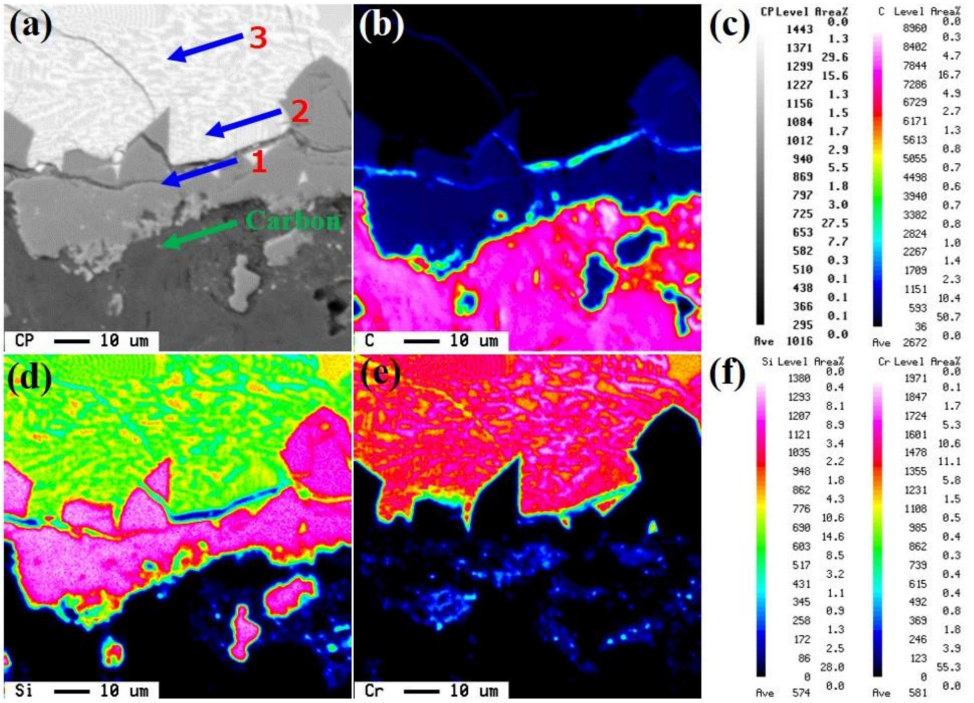

Fig. 6. Cross-sectional SEM (backscattered electron) images and EPMA elemental concentration mapping of the carbon crucible after experiments for 1 h at 1800 °C.

(max/min levels) of Si and Cr, respectively. The SiC interlayer, confirmed by EDS point analysis at the location marked with arrow 1 (see Table I), between the carbon crucible and solvent was found. The SEM (backscattered electron) images and EDS point analysis (see Table I) showed that after the experiment the solvent was divided into two types, Si-rich and Cr-rich zones. This was confirmed by EPMA mapping, as shownin Fig. 5.

TABLE I

Comparison of elementary compositions obtained from EDS point analysis corresponding to selected locations marked with arrows in Figs. 5 and 6.

Location		5 min	1 h
	1	SiC	SiC
2	Si [at%]	65.9	65.3
	Cr [at%]	34.1	34.7
3	Si [at%]	39.1	40.1
	Cr [at%]	60.9	59.9

As shown in Figs. 5 and 6, the Si concentration was significantly lower in the longer experiment, resulting in a relative increase in the Cr concentration. This decrease in Si concentration in the solvent might be due to Si being consumed by the crystallization of SiC.

Considering all the above results, the second increases in carbon content shown in Fig. 2 were due to the carbon crucible, which consisted of metastable phase carbon and was used as both the container and solute, causing crystallization of small SiC grains in the solvent after reaching saturation. Meanwhile, the constant carbon content probably resulted from an equilibrium between the SiC interlayer along the crucible wall and the solvent. Li *et al.* [13] demonstrated the mechanism of formation of the SiC interlayers between liquid silicon and solid carbon. A continuous SiC interlayer at the contact with carbon was formed by the reaction between liquid silicon and solid carbon during an isothermal hold. And a discontinuous SiC interlayer at the metal side was formed by the precipitation during a cooling process. According to their results, 1.64 μm of the continuous SiC interlayer, as shown in Fig. 5, was occupied by 4.8% of the measured carbon content. The clear separation between the continuous SiC and discontinuous SiC interlayer is impossible. Accordingly, the constant value in Fig. 2 was assumed to be slightly larger than the actual carbon solubility at SiC saturation in the solvent.

Figure 7 shows the experimentally obtained constant carbon contents in $Si_{0.6}Cr_{0.4}$ in the temperature range 1500–1950 °C for a duration of 5 min, represented as the closed spares. The carbon content increased with increasing temperature. The data of the calculated carbon solubility in $Si_{0.6}Cr_{0.4}$ solvent was provided from the Mitani research group [10]. The experimentally obtained carbon contents were compared with the solid line, which originated from phase diagrams of the Si–Cr–C systems calculated by Thermo-Calc (Thermo-Calc Software, Sweden) based on the CALPHAD method [10–12]. The thermodynamic dataset and Gibbs energy functions for Si, Cr, and C were obtained from the SGTE database (SSOL5) implemented in Thermo-Calc. The solid curve in the phase diagram in Fig. 7 shows the calculated carbon solubility in $Si_{0.6}Cr_{0.4}$ solvent. Even though the carbon content, including the SiC interlayer formed during the isothermal hold, was considered, the values measured in this study were in good agreement with the calculated

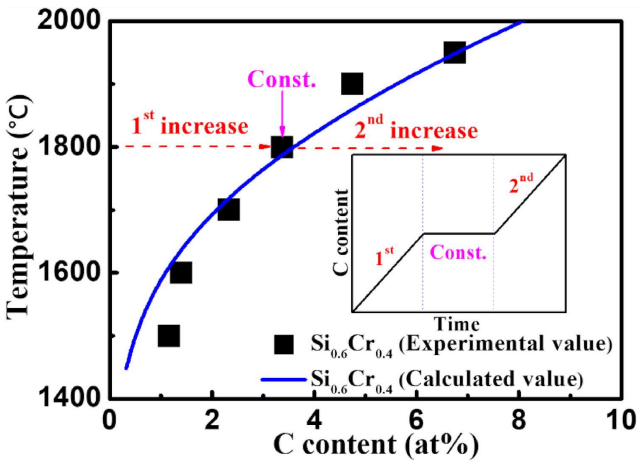

Fig. 7. Experimental and calculated values [10] of carbon solubility at various temperatures. Inset: Simplified illustration of results shown in Fig. 2.

carbon solubility, as shown in Fig. 7. Therefore, the constant carbon content can be considered to be close to the carbon solubility in the solvent at the given temperature. The inset of Fig. 7, a simplified illustration of the results in Fig. 2, suggests that the first and second increases in carbon content corresponded to the dotted arrows in Fig. 7, according to the pseudo binary phase diagram for the Si–C binary system.

4. Conclusion

In this study, the reaction between a carbon crucible and Si–Cr solvent, and carbon solubility in the solvent, were investigated using infrared absorption after combustion, FE-SEM, and EPMA. The carbon content initially increased for 5 min, then became constant until 10 min, and then increased again with time at high temperature. From the SEM and EPMA results, it was assumed that the second increase in carbon content was due to the crystallization of small SiC grains in the solvent after reaching saturation, and that the constant carbon content was due to the equilibrium between the SiC interlayer along the crucible wall and the solvent. The experimentally obtained constant carbon contents for $Si_{0.6}Cr_{0.4}$ at 1500–1950 °C was assumed to be closely represented the carbon solubility at each temperature, a pseudo binary phase diagram was created for Si and C. Even though the carbon content, including the SiC interlayer formed during the isothermal hold, was considered, the experimentally obtained constant carbon contents were in good agreement with the carbon solubility calculated using CALPHAD.

Acknowledgments

We would like to thank the Super Cluster Program of the Japan Science and Technology Agency (JST) for financial support. We also thank Dr. Takeshi Mitani and Dr. Naoyoshi Komatsu of the National Institute of Advanced Industrial Science and Technology (AIST) for

their kind support regarding CALPHAD carbon solubility calculations. We also wish to thank Mr. Satoshi Kobayashi and Mr. Yutaka Komatsu of Nagano Prefecture General Industrial Technology Center for their kind support regarding the measurement of EPMA and carbon contents using infrared absorption after combustion.

References

[1] X. Ding, J. Cheng, F. Chen, *Energies* **10**, 533 (2017).

[2] Y.M. Tairov, V.F. Tsvetkov, *J. Cryst. Growth* **43**, 209 (1978).

[3] K. Kamei, K. Kusunoki, N. Yashiro, N. Okada, K. Moriguchi, H. Daikoku, M. Kado, H. Suzuki, H. Sakamoto, T. Bessho, H. Sakamoto, T. Bessho, *Mater. Sci. Forum* **45**, 717 (2012).

[4] K. Kamei, K. Kusunoki, N. Yashiro, N. Okada, T. Tanaka, A. Yauchi, *J. Cryst. Growth* **311**, 855 (2009).

[5] K. Kusunoki, N. Okada, K. Kamei, K. Moriguchi, H. Daikoku, M. Kado, H. Sakamoto, T. Bessho, T. Ujihara, *J. Cryst. Growth* **395**, 68 (2014).

[6] K. Danno, H. Saitoh, A. Seki, H. Daikoku, Y. Fujiwara, I. Ishii, H. Sakamoto, Y. Kawai, *Mater. Sci. Forum* **13**, 645 (2010).

[7] S. Kawanishi, T. Yoshikawa, K. Morita, N. Okada, K. Kusunoki, K. Kamei, *J. Cryst. Growth* **381**, 121 (2013).

[8] C. Jacquier, G. Ferro, F. Cauwet, J.C. Viala, G. Younes, Y. Monteil, *J. Cryst. Growth* **254**, 123 (2003).

[9] O. Filip, B. Epelbaum, M. Bickermann, A. Winnacker, *J. Cryst. Growth* **271**, 142 (2004).

[10] T. Mitani, N. Komatsu, T. Takahashi, T. Kato, K. Fujii, T. Ujihara, Y. Matsumoto, K. Kurashige, H. Okumura, *J. Cryst. Growth* **401**, 681 (2014).

[11] A. Onuma, S. Maruyama, N. Komatsu, T. Mitani, T. Kato, H. Okumura, Y. Matsumoto, *Cryst. Growth Des.* **17**, 2844 (2017).

[12] L. Kaufman, H. Bernstein, *Computer Calculation of Phase Diagrams*, Academic Press, New York 1970.

[13] J.G. Li, H. Hausner, *J. Am. Ceram. Soc.* **79**, 873 (1996).